Concurrent extreme events of atmospheric moisture transport and precipitation: the role of atmospheric rivers.

Luis Gimeno-Sotelo [a,*], Luis Gimeno[a]

[a] *Centro de Investigación Mariña, Universidade de Vigo, Environmental Physics Laboratory (EPhysLab), Ourense, Spain*

Abstract

An analysis of concurrent extreme events of precipitation and Integrated Water Vapour Transport (IVT) is crucial to our understanding of the role of the major global mechanisms of atmospheric moisture transport, including that of the Atmospheric Rivers in extratropical regions. The aim herein is to analyse how IVT depends on precipitation at each point on a worldwide grid, separately for each season. For this purpose, gridded data on CPC precipitation and ERA-5 IVT at a spatial resolution of 0.5° were used, covering the period from Winter 1980/1981 to Autumn 2017. For each season, and for each point with more than 400 non-dry days, several copula models were fitted to model the joint distribution function of the two variables. At each of the analysed points , the best copula model was used to estimate the probability of a concurrent extreme of the two variables. At the same time, within the sample of observed concurrent extremes, the proportion of days with Atmospheric Rivers (ARs) was calculated for the whole period and for two 15-year sub-periods, one earlier period and one more recent (warmer) period. Three metrics based on copulas were used to analyse carefully the influence of IVT on extreme precipitation in the main regions of occurrence of AR landfall. The results show that the probability of occurrence of concurrent extremes is strongly conditioned by the

*Corresponding author
Email address: luis.gimeno-sotelo@uvigo.es (Luis Gimeno-Sotelo)

dynamic component of the IVT, the wind. The occurrence of ARs accounts for most of the concurrent extreme days of IVT and precipitation, with percentages of concurrent extreme days close to 90% in some seasons of the year in almost all the known regions of maximum occurrence of ARs, and with percentages greater than 70% downwind of AR landfall regions. This coincidence was lower in tropical regions, and in monsoonal areas in particular, with percentages of less than 50%. With a few exceptions, the role of ARs as drivers of concurrent extremes of IVT and precipitation tends to show a decrease in recent (warmer) periods. For almost all the AR regions with high or very high probabilities of achieving a concurrent extreme of IVT and precipitation, there is a general trend towards a lower influence of IVT on extreme precipitation in recent (warmer) periods.

Keywords: Extreme precipitation, Moisture transport, Atmospheric Rivers, Concurrent extremes, Copulas

1. Introduction

Atmospheric moisture transport is the essence of the atmospheric branch of the hydrological cycle, and has crucial importance in precipitation on the continents, in terms of both its average values (Gimeno et al., 2010, 2012, 2020; van der Ent et al., 2010; van der Ent & Savenije, 2013) and its extremes (Vázquez et al., 2020; Liu et al., 2020; De Vries, 2021). Any intensification (or reduction) in transported moisture results in precipitation anomalies and flooding (or drought) when these are high (or low) (Gimeno et al., 2016; Drumond et al., 2019; Liu et al., 2020). The role of moisture transport is even more important in extreme precipitation. According to a simple approximation, extreme precipitation scales with moisture content and with some indicator of atmospheric instability, being much more sensitive to the former (Emori & Brown, 2005; Nie et al., 2018). Extreme precipitation requires a certain threshold of atmospheric instability, once it is reached the value of extreme precipitation increases as the water vapour content increases (Emori & Brown, 2005; Kunkel et al., 2020). In

order to maintain high moisture in the atmospheric column, a constant supply of humidity from outside is required, in other words, high moisture transport. The relationship between moisture transport, moisture content, and extreme precipitation must therefore be intense and of great importance, not just in hydro-meteorological terms, but also in terms of climate change, because the three parameters all scale approximately with temperature following a thermodynamic constraint imposed by the Clausius-Clapeyron equation (Held & Soden, 2006; Bao et al., 2017) ; specifically, they grow around 6-7% for each degree of increase in atmospheric surface temperature.

If moisture transport is quantified as vertically integrated water vapour transport (IVT), a local measure of the moisture advected horizontally in the atmosphere, the extremes values of IVT and precipitation should occur simultaneously at grid scale. This simultaneous occurrence must be spatially and temporally heterogeneous throughout the world because most of the moisture is transported via two major mechanisms of atmospheric moisture transport, Low Level Jets (LLJs) in tropical and subtropical regions and Atmospheric Rivers (ARs) in subtropical and extratropical areas (Gimeno et al., 2016). The first of these structures, LLJs, have semi-permanent positions with well defined but distant moisture sources, regions of IVT maxima, and moisture sinks, where the precipitation associated with the system is the highest (Algarra et al., 2019). The distance between areas of strong IVT and precipitation associated with LLJs means that the influence that IVT should have on extreme precipitation (at grid scale) may not be that strong. This problem of distance is not seen in the other major mechanism of moisture transport, ARs, which are non-permanent narrow and long corridors of moisture in the atmosphere (Zhu & Newell, 1994; Gimeno et al., 2014; Ralph et al., 2018). ARs are generally, though not always, associated with extratropical cyclones (Gimeno et al., 2021) , and are characterised and even frequently defined by high values of IVT (Neiman et al., 2008). They are closely related to heavy precipitation associated mainly with baroclinic development and orographic forcing (Ralph et al., 2006; Ralph & Dettinger, 2011; Ralph et al., 2016; Tan et al., 2021; Dettinger et al., 2015; Gimeno

et al., 2014; Mukherjee & Mishra, 2021a). AR occurrence shows intraseasonal variations and preferential areas of occurrence (Guan & Waliser, 2015; Algarra et al., 2020), therefore in the areas and preferred seasons of AR occurrence, a very high occurrence of concurrent extremes of IVT and precipitation may be expected. In this context, the analysis of those concurrent extremes is of crucial importance in understanding the role of the ARs as a major mechanism behind precipitation extremes.

The analysis of concurrent extremes, defined as the simultaneous occurrence of extreme values of at least two variables, is a topic of recent and intense interest. Most studies have focused on variables whose extreme joint occurrence is linked with natural hazards, such as storm surges and heavy precipitation (e.g. Wahl et al., 2015; Bevacqua et al., 2019) , droughts and heatwaves (e.g. Mazdiyasni & AghaKouchak, 2015) , or precipitation and extreme wind (e.g. Martius et al., 2016; Zscheischler et al., 2021). A more meteorological derivation of these phenomena implies an understanding of the role of specific meteorological systems in the genesis of these concurrent extremes, hence the existence of various studies of the relationship between concurrent wind and precipitation and extratropical cyclones (e.g. Owen et al., 2021 for Europe or Messmer & Simmonds, 2021 at a global scale), with fronts only or with combined cyclones and fronts (Catto & Dowdy, 2021). The present study is set against this conceptual background of concurrent extremes.

In our present investigation we will make use of copulas in order to model the joint distribution function of IVT and precipitation. This is very common in environmental research (see e.g., Cong & Brady, 2012; Reddy & Ganguli, 2012; Zscheischler & Seneviratne, 2017; Lazoglou & Anagnostopoulou, 2019). Our analysis is carried out at each point on a global grid, separately for each season. At each analysed point, the best copula model is used to estimate the probability of a concurrent extreme of the two variables. Furthermore, within the sample of observed concurrent extremes, the proportion of days with ARs is also calculated. For those regions with the highest occurrence of landfalling ARs, we also use copula models to estimate the conditional probability of achieving

an extreme precipitation event for a given value of IVT, and the IVT value for a given conditional probability of extreme precipitation.

The aim of the present study is to gain an insight of the role of ARs in the occurrence of concurrent extreme events of atmospheric moisture transport and precipitation. One previous study is relevant and merits special attention. Waliser & Guan (2017) estimated the impact of ARs on extremes of 10-m wind and precipitation and found, among other results of note, that ARs are associated with about 50% of concurrent extremes across most mid-latitude regions. IVT is the variable we use to compute moisture transport, and while this depends on wind it also depends on moisture, and furthermore it is computed for the whole vertical column and not just at 10 m. There are many other differences between our study and that of Waliser & Guan (2017), both methodological (e.g., our use of copulas to deal with concurrent extremes) and conceptual (e.g., we focus on the role of the extremes of IVT, which provide high values of moisture content and are thus related to extreme precipitation). Their results are nevertheless of great interest in comparison with ours.

2. Data

IVT and precipitation. We obtained daily IVT and precipitation data at a spatial resolution of 0.5° for the period 1981-2017. Precipitation data were obtained from the Climate Prediction Center Global Unified Gauge-Based Analysis (CPC) (Xie et al., 2007). CPC is a gauge-based product, which assimilates daily reports from more than 30,000 stations, and uses an optimal interpolation algorithm that accounts for orography. CPC is well known to have the advantage of a high station density with any limitations in the gauge network density, which is poor over tropical Africa and Antarctica. IVT, as defined in (1), was calculated from data obtained from the European Centre for Medium-Range Weather Forecasts Reanalysis ERA-5 (Hersbach et al., 2020), where q is the specific humidity, $\mathbf{U}$ is the horizontal wind field, and Ω refers to the integration

over the whole tropospheric column.

$$IVT = \frac{1}{g}\left|\left(\int_{\Omega} q\mathbf{U}dp\right)\right| \tag{1}$$

The CPC data set was based on station reports plus interpolation, and has an important advantage compared with the use of precipitation obtained directly from ERA-5 reanalysis. Because our aim is to study the simultaneous occurrence of extremes of IVT and precipitation, and the former is calculated from the reanalysis, the use of precipitation data also obtained from the reanalysis could result in a concurrent extreme due partly to the use of the same model to construct the reanalysis. The selection of ERA-5 to calculate IVT rather than any other reanalysis is because of the well-known reliability of the reanalysis produced by the European Centre for Medium-Range Weather Forecasts for hydrological applications (e.g., Xu et al., 2019; Tarek et al., 2020). Figure 1 shows the total number of days with non-zero precipitation at each grid point for December-January-February (top) and June-July-August (bottom) and Figure S1 for intermediate seasons (March-April-June and September-October-November). The annual precipitation frequency map (not shown) visually compares well with previous analogous maps by Sun et al. (2006, their Fig. 1) and Beck et al. (2019, their Fig. 8a).

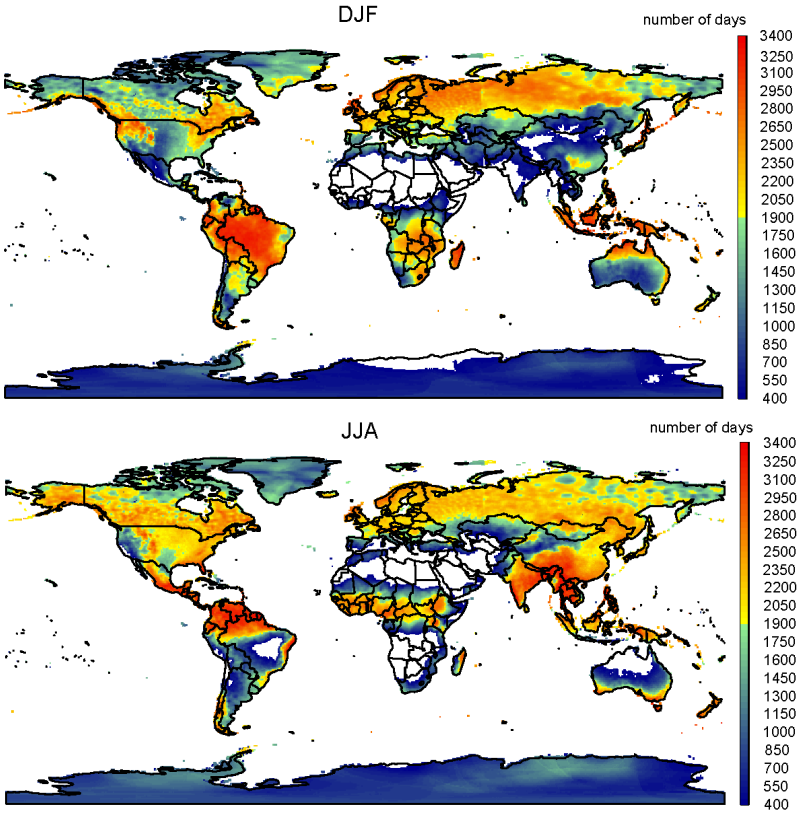

Figure 1: Total number of days for the period 1981-2017 with non-zero precipitation at each grid point for December-January-February (top) and June-July-August (bottom).

Occurrence of ARs. The daily occurrence of ARs for each continental 0.5° grid point for the period 1981-2017 was estimated from the AR database developed by Guan & Waliser (2015). This database applies thresholds of IVT intensity and geometric conditions to ERA-Interim reanalysis data (Dee et al., 2011) to identify the locations of ARs at a global scale. Because the spatial resolution of this database is 1.5°, all the 0.5° grid-points included in any 1.5° grid-point considered as an AR were also considered in the same way. Figure 2 shows the total number of occurrences of ARs at each grid point for December-January-February (top) and June-July-August (bottom), and Figure S2 shows the same data for intermediate seasons March-April-June and

September-October-November. The plots show the known occurrence of ARs, with maxima in the extratropical North Atlantic/Pacific, southeastern Pacific, and South Atlantic, and the most frequent landfalling ARs along the west coasts of Europe, North America, and southern South America (Guan & Waliser, 2015; Algarra et al., 2020).

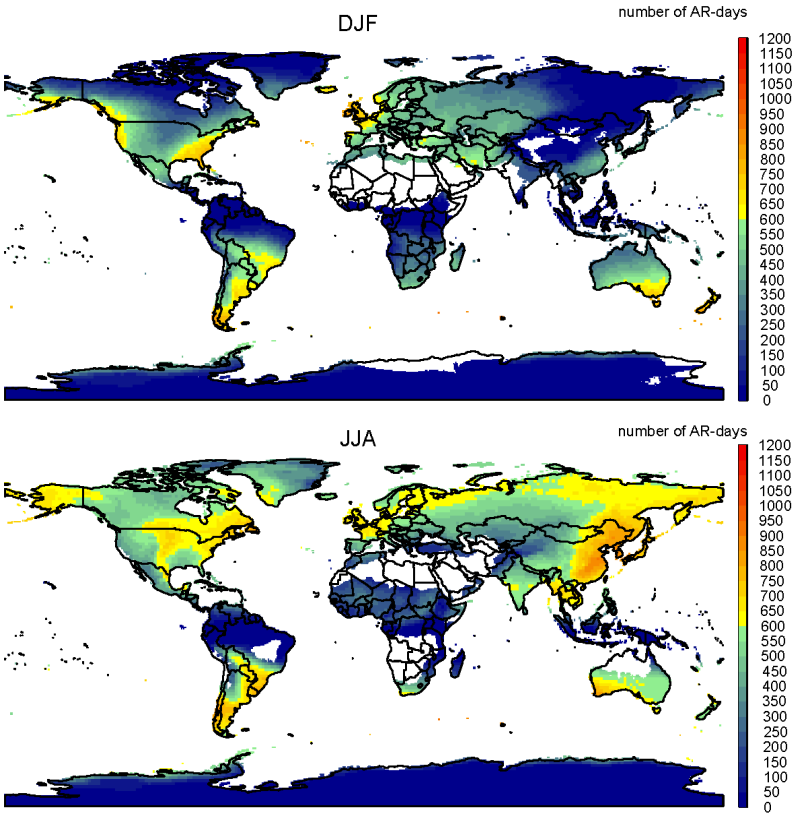

Figure 2: Number of days of occurrence of ARs for the period 1981-2017 at each grid point, for December-January-February (top) and June-July-August (bottom).

3. Methods

As noted in Section 1, the statistical analysis in this study is based on **copula theory**. A comprehensive description of this theory is given in Nelsen (2006),

Joe (2014) and Shemyakin & Kniazev (2017). We now present a brief summary of some of the most pertinent aspects.

The concept of copula. Let (U, V) be a random pair with U and V following a uniform distribution with a mean of 0 and a standard deviation of 1. A copula C is its joint distribution function, i.e.:

$$C(u, v) = P(U \leq u, V \leq v), \quad u, v \in (0, 1). \tag{2}$$

For two continuous variables X and Y with arbitrary distribution functions F and G respectively, the joint distribution function of (X, Y), denoted by H, can be written as a function of a copula and the marginal distributions, according to **Sklar's Theorem** (Sklar (1959)):

$$H(x, y) := P(X \leq x, Y \leq y) = C(F(x), G(y)), \quad x, y \in \mathbb{R} \tag{3}$$

In our case F and G will be estimated non-parametrically (the corresponding empirical distribution functions will be used), therefore the choice of an appropriate model for the copula C results directly in a model for the joint distribution H.

Copula models. The copula models used here belong to the Elliptical and Archimedian families.

Regarding **Elliptical** copulas, Gaussian and Student-t types will be used:

- *Gaussian copula*:

$$C(u, v; \rho) = \Phi_\rho(\Phi^{-1}(u), \Phi^{-1}(v)), \quad u, v \in (0, 1), \tag{4}$$

  where $\Phi^{-1}(.)$ is the inverse of the distribution function of a standard normal distribution and $\Phi_\rho(., .)$ is the joint distribution function of a standard bivariate normal distribution with Pearson's linear correlation coefficient ρ.

- *Student-t copula*:

$$C(u, v; \eta, \rho) = T_{\eta\rho}(T_\eta^{-1}(u), T_\eta^{-1}(v)), \quad u, v \in (0, 1), \tag{5}$$

where $T_\eta^{-1}(.)$ is the inverse of the distribution function of the Student-t distribution with η degrees of freedom and $T_{\eta\rho}(., .)$ is the joint distribution function of a bivariate Student-t distribution with η degrees of freedom and Pearson's linear correlation coefficient ρ.

With respect to the **Archimedian** copulas used in this article, Table 1 lists the expressions of the models.

Table 1: Archimedian copulas used in this article.

Model	C(u,v)	$\alpha \in$
Frank	$-\frac{1}{\alpha}\log\left(\frac{1-e^{-\alpha}-(1-e^{-\alpha u})(1-e^{-\alpha v})}{1-e^{-\alpha}}\right)$	$\mathbb{R}\setminus\{0\}$
Gumbel	$\exp\left[-\{(-\log(u))^\alpha+(-\log(v))^\alpha\}^{1/\alpha}\right]$	$[1,\infty)$
Clayton	$\max\left\{\left(u^{-\alpha}+v^{-\alpha}-1\right)^{-1/\alpha}, 0\right\}$	$[-1,\infty)\setminus\{0\}$
Joe	$1-[(1-u)^\alpha+(1-v)^\alpha-(1-u)^\alpha(1-v)^\alpha]^{\frac{1}{\alpha}}$	$[1,\infty)$

The *independence copula* will also be used:

$$C(u, v) = uv, \quad u, v \in (0, 1). \tag{6}$$

Using copulas to study concurrent extremes. Let $U = F(X)$ and $V = G(Y)$ be the uniform-transformed random variables and (u, v) the bivariate threshold (on the uniform scale). In order to analyse the joint extremal behaviour of the variables in our study, we focus on the probability that both variables exceed the corresponding threshold (see Salvadori & De Michele, 2004):

$$p_{AND} = P(U > u, V > v) = 1 - u - v + C(u, v) \tag{7}$$

We also make use of the conditional probability of one variable exceeding a threshold, given a fixed value of the other variable. This has the following expression (Salvadori & De Michele, 2004):

$$p_{COND} = P(V > v|U = u) = 1 - \frac{\partial}{\partial u} C(u, v) \tag{8}$$

Parameter estimation. Let us consider an observed sample $((x_1, y_1), ..., (x_n, y_n))$ of the studied pair (X, Y). The question is then of how this information can be used to estimate the parameters of the copula models. There are several methods of estimation (see Joe, 2014; Shemyakin & Kniazev, 2017), and in this article our analysis will be based on the **semi-parametric** approach:

1. Pseudo-observations $\{(\hat{u}_i, \hat{v}_i), i = 1, 2, ..., n\}$ are computed, where $\hat{u}_i := \frac{n}{n+1}\widehat{F}(x_i)$ and $\hat{v}_i := \frac{n}{n+1}\widehat{G}(y_i)$, with $\widehat{F}$ and $\widehat{G}$ being the empirical distribution functions of X and Y, respectively.

2. The resulting estimator, the Maximum Pseudo-Likelihood Estimator (MPLE), can be calculated as follows: $\widehat{\underset{\sim}{\theta}} = \text{argmax} \sum_{i=1}^{n} \log(c(\hat{u}_i, \hat{v}_i)|\, \underset{\sim}{\theta})$, where $\underset{\sim}{\theta}$ is the parameter vector of the copula model and $c(.,.)$ is the copula density function, defined as $c(u, v) = \frac{\partial^2 C}{\partial u \partial v} = \frac{\partial^2 C}{\partial v \partial u}, \quad u, v \in (0, 1)$.

4. Results and discussion

4.1. Worldwide analysis of concurrent extremes

The copula models presented in Section 3 were fitted to the IVT and precipitation data introduced in Section 2. That is, for each season (December-January-February, March-April-May, June-July-August, September-October-November), we fitted for each grid point with more than 400 days of non-zero precipitation the following copula models to the pair (IVT,precipitation): a Gaussian, a Student-t, a Frank, a Gumbel, a Clayton, a Joe and an independence copula. We chose to consider only those grid points because a sample size of more than 400 bivariate observations allowed us to work comfortably with copulas. For

the parameter estimation, we used the semi-parametric approach explained in Section 3. Among those copula models that were fitted, only the best one according to the AIC (Akaike, 1974) was considered for our analysis (the one with the lowest AIC value). In Figure 3 it is possible to see the best fitted copula model for the pair (IVT,precipitation) at each grid point, for December-January-February (top) and June-July-August (bottom). Regarding the intermediate seasons (March-April-June and September-October-November), this information can be found in Figure S3.

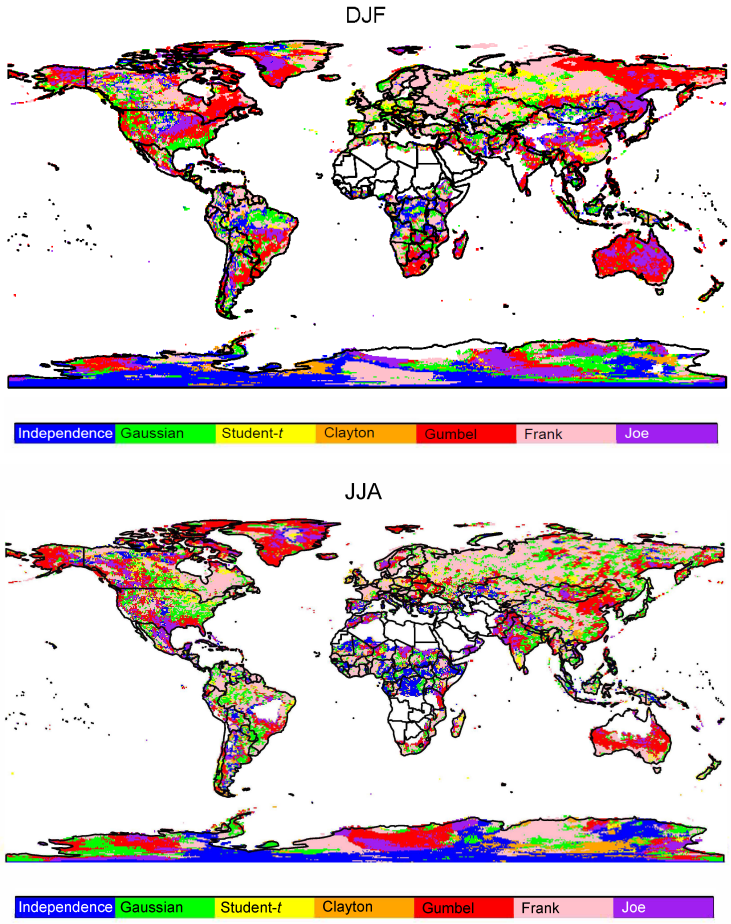

Figure 3: Fitted copula type with the lowest AIC value for December-January-February (top) and June-July-August (bottom).

The simplest way of defining concurrent extremes of two variables (in our case IVT and precipitation) involves counting the number of days on which a quantile-based threshold for the two variables is exceeded, in our case this is the 90th percentile (Figure 4 for December-January-February (top) and June-July-August (bottom) and supplementary Figure S4 for intermediate seasons). The general distribution of number of concurrent extremes seems to show that it is highly conditioned by the dynamic component of the IVT, the wind (Martius

et al., 2016). Values are low in the deep tropics, where precipitation is mainly convective, and not favoured by strong horizontal winds and moisture transport. The number of concurrent extremes shows an increase in extratropical regions, reaching higher values along the coast of the continents. Precipitation over these regions is derived mainly from extratropical cyclones, characterized simultaneously by high winds, and therefore strong moisture transport, and precipitation (Messmer & Simmonds, 2021). Baroclinic activity is more intense during winter, and consequently the number of concurrent extremes is higher in extratropical regions in the corresponding winter than in summer. This general pattern is disturbed regionally by the action of meteorological structures associated with strong moisture transport, in which high humidity is combined with low-level wind. Examples of this are the high values of concurrent extremes in the NE Brazilian region in JJA affected by Low-Level Jet (LLJ) systems (Braz et al., 2021), or the moderate values in the SE of North America in JJA affected by tropical cyclones (Liu et al., 2021). To sum up, maxima of concurrence of extremes are found on extratropical continental coasts during winter, mostly affected by ARs with regional fingerprints of other major mechanisms of atmospheric moisture transport such as LLJs or tropical cyclones. The absolute number of concurrent extremes is in part dependent on the number of precipitation days (Figures 1 and S1) because IVT occurs every day, so the presence of low values in the tropics, where the number of precipitation days is very high, implies a very low extremal dependence. For extratropical latitudes over the Northern Hemisphere with many precipitation days, a very high number of concurrent extremes may not mean that the extremal dependence is so high. At this point, therefore, it is interesting to know the geographical distribution of the values of the 90th percentiles of IVT and precipitation.

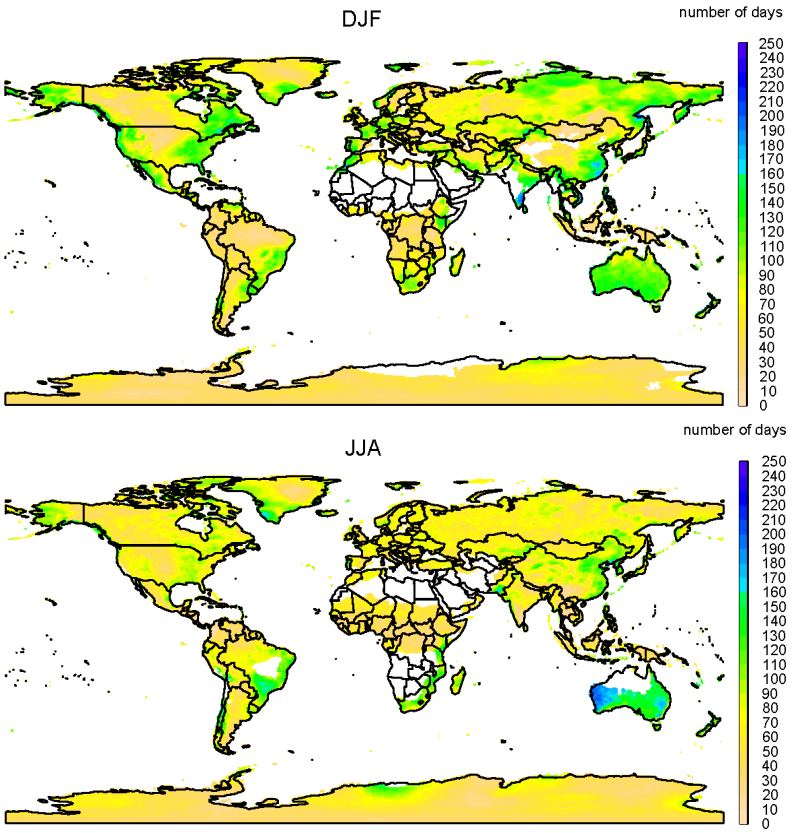

Figure 4: Number of days exceeding the bivariate threshold ($q90_{IVT}$, $q90_{prec}$) for December-January-February (top) and June-July-August (bottom) for the period 1981-2017.

Figure 5 shows the 90th percentile values of IVT ($q90_{IVT}$) for December-January-February (top) and June-July-August (bottom) (values for intermediate seasons are shown in Figure S5). The global distribution reveals low values over the polar regions and areas with high topography, and high values over tropical and extratropical coasts dominated by tropical easterlies and storm tracks. A more detailed inspection of the regions of maximum occurrence reveals that these regions coincide with the main areas of occurrence of ARs, such as the Californian or Western European coasts and the main LLJ systems, as clearly seen in the Great Plains in North America or along the Andes in South

America (Gimeno et al., 2016; De Vries, 2021). However, and as expected, the absolute maxima are linked to the Asian monsoon in the wet season (JJA). It is also clear that in extratropical regions in the Northern Hemisphere, extreme values of IVT are lower for the Pacific than for the Atlantic coasts, with a clear contrast between the American Pacific coast and the American and European Atlantic coasts, which are three of the most important regions of occurrence of ARs. This is the case for both summer and winter. In the Southern Hemisphere, higher extreme values of IVT occur on the Australian coasts than on the South African or Chilean coasts, even though all three are at similar latitudes.

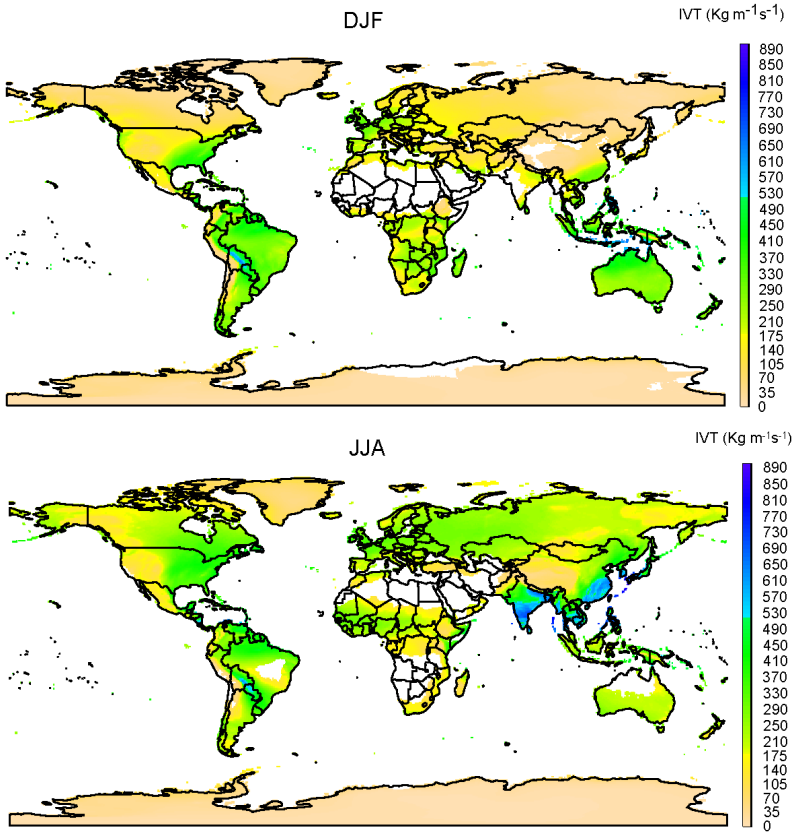

Figure 5: 90th percentile of IVT for December-January-February (top) and June-July-August (bottom) for the period 1981-2017.

Figure 6 shows the 90th percentile of daily precipitation ($q90_{prec}$) for December-January-February (top) and June-July-August (bottom) (intermediate seasons are shown in Figure S6). The annual distribution of $q90_{prec}$ (not shown) is visually comparable with previous equivalent maps by Dietzsch et al. (2017, their Fig. 5c and 5d) and Beck et al. (2019, their Fig. 7a) . In general, the pattern is quite similar to annual mean precipitation, with maximum values along the Intertropical Convergence Zone (ITCZ), varying seasonally with its movement, and over monsoonal regions during the wet season. Secondary maxima occur in regions of extra-tropical cyclone tracks on North-west American or European west coasts during the boreal winter or on the coasts of New Zealand and Chile during the austral winter. Areas of occurrence of other meteorological systems that produce extreme precipitation events are also identified as local maxima in Figure 6, such as areas of occurrence of tropical cyclones (e.g., on the North American east coast during boreal summer) or Mesoscale Convective Systems (e.g., the Plata river basins during the austral winter). The large area of high $q90_{prec}$ over the Amazon region is in part due to high values over the region but is also partly due to the limited number of precipitation gauges, implying a loss of variance due to the effects of interpolation (Haberlandt, 2007).

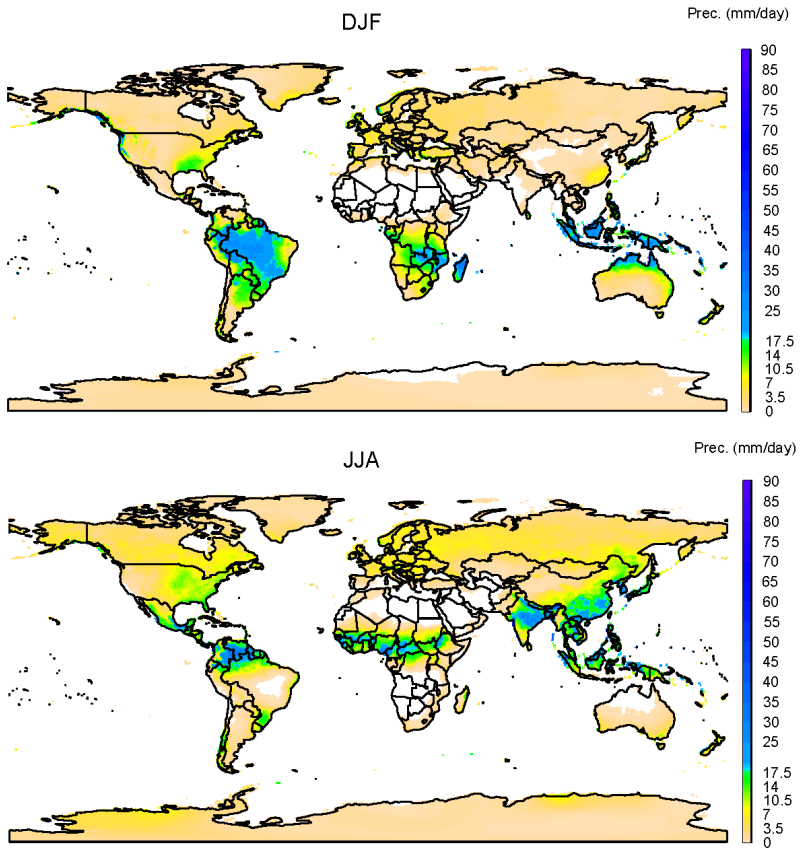

Figure 6: 90th percentile of precipitation for December-January-February (top) and June-July-August (bottom) for the period 1981-2017.

The spatial distribution of concurrent extremes shown in Figure 4 is related partly to the local number of precipitation days, so it is convenient to estimate the probability of achieving a concurrent extreme of IVT and precipitation. This is shown in Figure 7 for December-January-February and June-July-August and in Figure S7 for intermediate seasons. In the figure, we show both the "empirical probability", which refers to the percentage of concurrent extremes with respect to the number of days with nonzero precipitation, and the copula-based probability, which was computed according to (7) using the copula model

with the lowest AIC value for each grid point. On first inspection, it appears that the two plots are more-or-less coincident, which gives high confidence in the copula models selected grid-by-grid. With the exception of regions of occurrence of ARs, monsoonal areas, and regions influenced by LLJs, the probability of joint extremes is less than 4%. The general distribution of maxima of probability resembles the number of concurrent extremes, but there are some differences linked mostly to the number of precipitation days. Therefore, maxima of around 40% of probability are shown in monsoonal areas during the dry season. This effect is particularly visible in DJF for the Asian and North American monsoonal regions, and in JJA for the Australian and South America monsoonal regions, although it is also visible with a lower intensity for the African monsoonal regions. Another effect of accounting for the number of days of precipitation is observed in the north-south gradient of probability in regions of occurrence of ARs. Thus, for DJF on the Atlantic- European-North African coasts there is a decrease in probability from values of the order of 25% on the Moroccan coasts to 4% on the Scandinavian ones. A similar decrease is seen on the American Pacific coast from California to Northern Canada. Maxima of probability are again evident in polar regions of ARs, with values higher than 25% in the Antarctica in JJA and somewhat lower, of the order of 8%, in Alaska and Kamchatka in DJF.

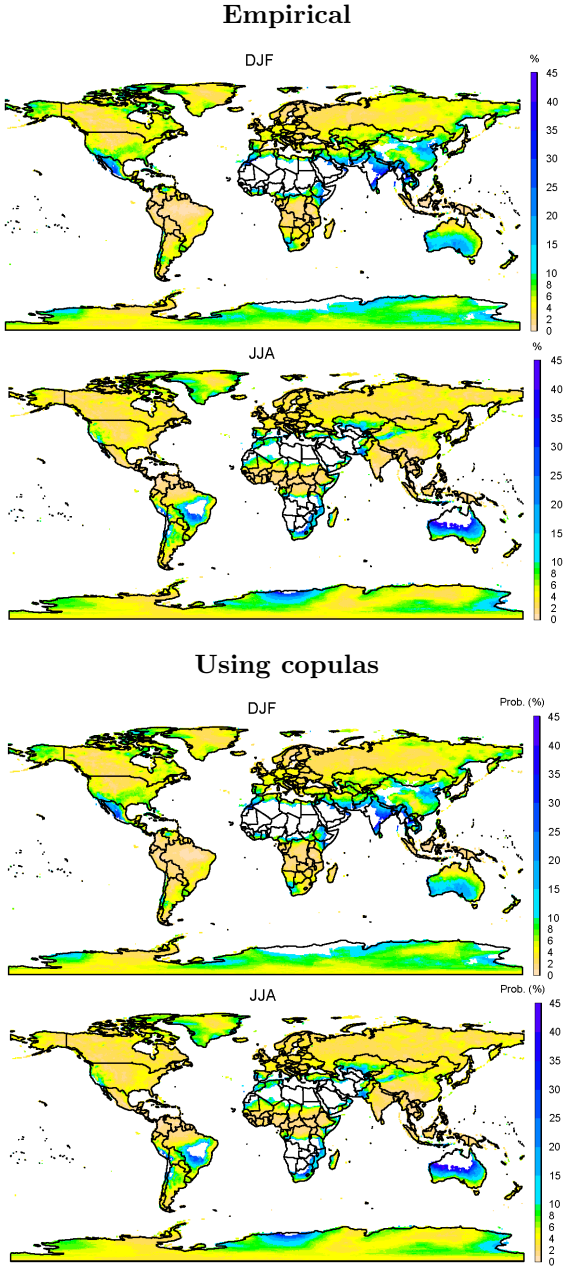

Figure 7: Estimated probability of achieving a concurrent extreme of IVT and precipitation (percent), for December-January-February and June-July-August for the period 1981-2017. The "empirical probability" refers to the percentage of concurrent extremes with respect to the number of days with non-zero precipitation. The copula-based probability is computed using the copula model with the lowest AIC value for each grid point.

A joint analysis of Figures 4 and 7, which account for the concurrent extremes and their probability, and Figures 5 and 6, which account for the thresholds of IVT and precipitation used to define their extremes, reveals regions with very high values of both IVT and precipitation, where the probability of occurrence of concurrent extremes is very low, such as the ITCZ or monsoonal regions in the wet season. On the other hand, there are regions with a high probability of concurrent extremes but with low values of IVT and precipitation, such as the polar regions or the monsoonal regions in the dry season. Moderate-to-high probabilities of occurrence of concurrent extremes accompanied by moderately high values of IVT and precipitation occur mainly in the areas of occurrence of ARs (Figure 2). We focus on these regions in the next section.

4.2. AR regions: concurrent extremes and conditional probabilities.

Figure 8 shows the percentage of concurrent extreme days of IVT and precipitation that coincide with the occurrence of ARs, for December-January-February, for the whole period 1981-2017, and for two 15-year sub-periods, an earlier period and a more recent warmer period , in order to investigate the potential effects of recent warming. Figure 9 and Figures S8 and S9 are the equivalent to Figure 8 for June-July-August, March-April-May and September-October-November respectively. In many studies, the period covered by reanalysis has been split in order to study differences between them based on the idea that the period since 2001 has been considerably warmer than the preceding period, 1980-2000 (a detailed justification of this approach with ERA5 data is shown in Mukherjee & Mishra (2021b)). Because the ENSO greatly affects the transport of moisture (Castillo et al., 2014; Kim et al., 2019; Xiong & Ren, 2021) , in order to define the two sub-periods we have removed the 6 years of strongest ENSO for each season (the 3 most intense El Niño and the 3 most intense La Niña according to the Extended Multivariate ENSO Index and available at https://psl.noaa.gov/enso/climaterisks/years/top24enso.html).

Therefore, for **December-January-February**, the *earlier period* corresponds to: 1981, 1982, 1984, 1985, 1986, 1987, 1988, 1990, 1991, 1993, 1994,

1995, 1996, 1997 and 1999 ; and the *later period* to: 2002, 2003, 2004, 2005, 2006, 2007, 2008, 2009, 2010, 2012, 2013, 2014, 2015, 2016 and 2017.

In the case of **June-July-August**, the *earlier period* refers to: 1981, 1982, 1984, 1985, 1986, 1990, 1991, 1992, 1993, 1994, 1995, 1996, 1998, 1999 and 2000; and the *later period* to: 2002, 2003, 2004, 2005, 2006, 2007, 2008, 2009, 2011, 2012, 2013, 2014, 2015, 2016 and 2017.

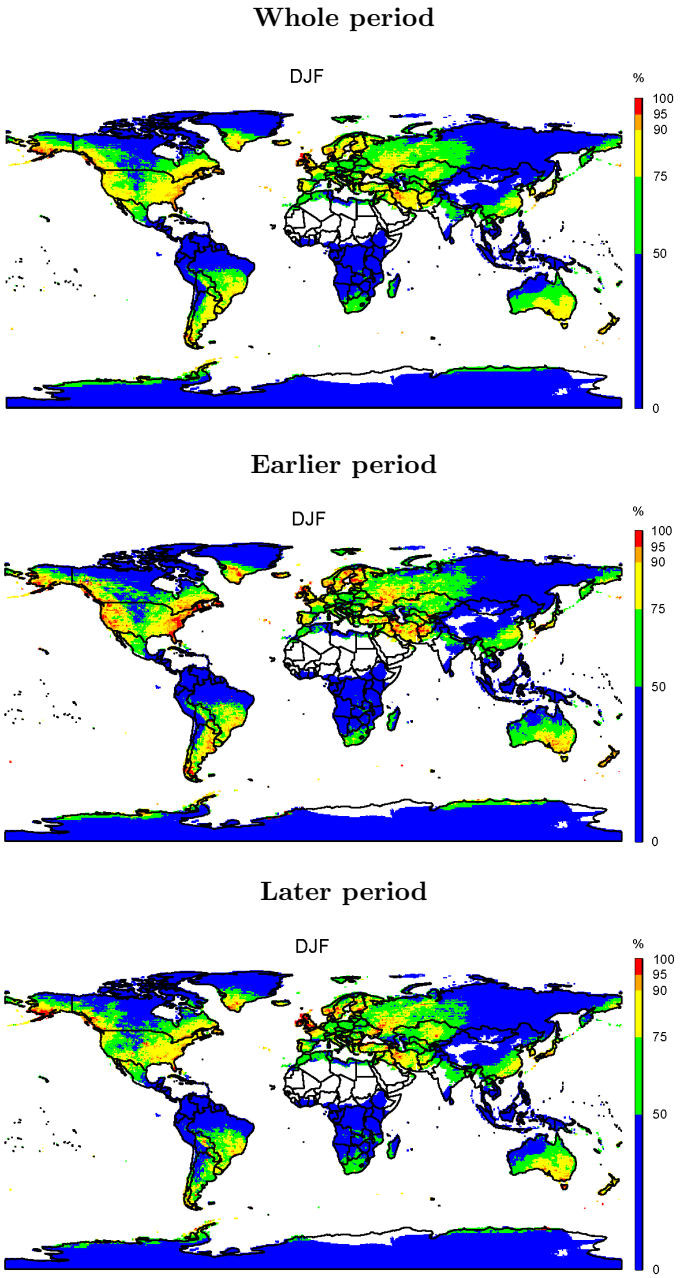

Figure 8: Percentage of concurrent extreme days of IVT and precipitation that coincide with the occurrence of ARs, for **December-January-February**, for the whole period 1981-2017, and the earlier and later studied periods.

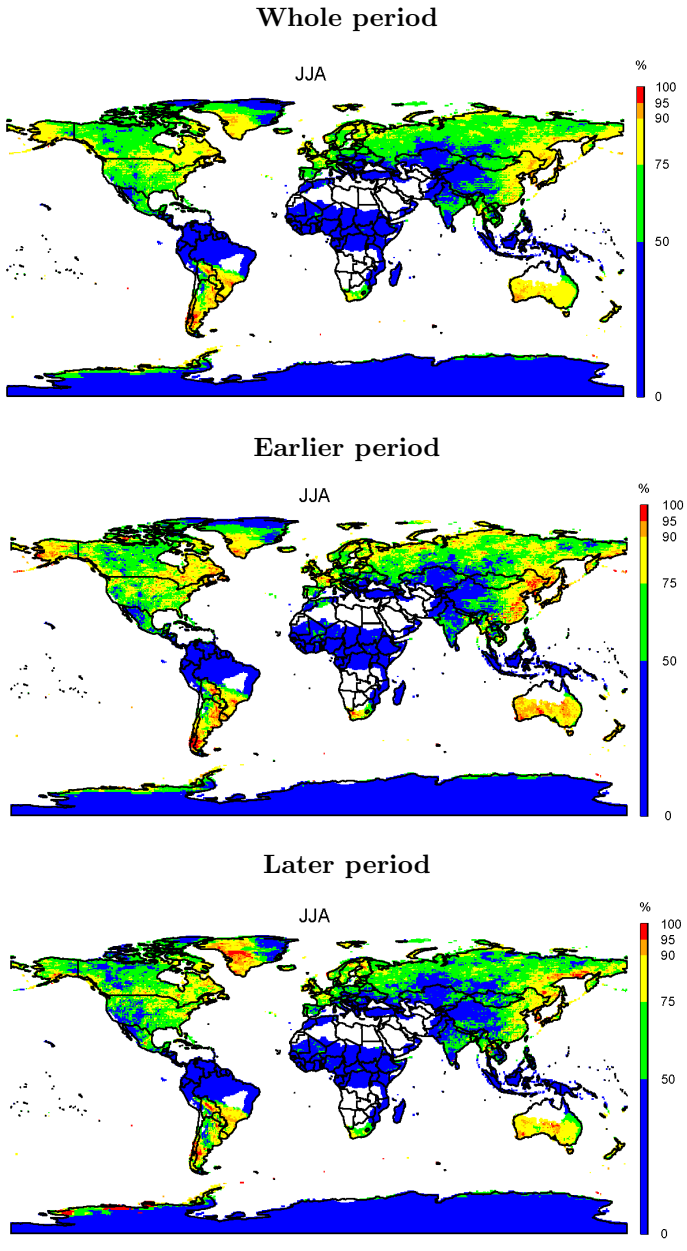

Figure 9: Percentage of concurrent extreme days of IVT and precipitation that coincide with the occurrence of ARs, for **June-July-August**, for the whole period 1981-2017, and the earlier and later studied periods.

Considering the whole period, percentages lower than 50% occur in tropical regions and over the Asian plateaus, and are higher in practically all extratropical and polar regions. Percentages higher than 90% occur in some seasons of the year in all the known regions of maximum occurrence of ARs, the North American Pacific, the European Atlantic, the Asian Pacific, the Southern Australian, South African, and South American coasts. Large continental regions downwind of these regions of preferential occurrence of ARs show percentages greater than 70%, reflecting the effect on inland penetration of ARs (Rutz et al., 2015; Lavers & Villarini, 2015; Nayak & Villarini, 2018; Ralph et al., 2019; Eiras-Barca et al., 2021). There are no percentages higher than 50% in any season in the monsoon regions, where the concurrence between IVT and precipitation is high, showing that in these regions both the definition of ARs and their effects are diffuse (Gimeno et al., 2021). In both hemispheres, the percentage is higher in autumn and winter than in spring and summer, with the exception of the Asian Pacific coasts. There are regions such as Iran where the concurrence of extreme IVT and precipitation is moderate or low but the percentage that coincide with ARs is high, reaching values close to 90% in spring and winter, and other regions such as the Antarctic around zero longitude where the opposite applies. A comparison with Waliser & Guan (2017), who used the same AR database, shows a high concordance in the regions they found with a high proportion of separate wind extremes and precipitation extremes associated with ARs, although with lower percentages in their study, partially due to their use of a more restrictive 98th percentile as the threshold for defining extremes.

The differences in the percentage of concurrent extreme days of IVT and precipitation that coincide with the occurrence of ARs between the earlier and more recent periods seem to reflect a spatially asymmetric variation. The general trend is towards a decrease in recent (warmer) periods, with a reduction in the percentage over the Pacific and Atlantic North American coasts (which is very marked during winter) and in the Southern Hemisphere regions (also more evident in the austral winter). There is no apparent change for the Pacific Asian coasts, and a slight regional increase on the European Atlantic coasts (e.g.,

British Isles in winter and the Iberian Peninsula in autumn). Although there could be factors other than warming and the ENSO (partially excluded from this study) that differentiate earlier and later sub-periods (for instance there was a change in the Atlantic Multidecadal Oscillation (AMO) phase from negative to positive in the mid-nineties; see Trenberth et al., 2021), the results point to a slight reduction with warming of the role of ARs as mechanism behind the concurrent extremes of IVT and precipitation. There are some physical factors that support this hypothesis. Although the number of ARs and the moisture transported by them is predicted by models to increase with warming (Espinoza et al., 2018; Massoud et al., 2019; Payne et al., 2020), the IVT associated with ARs increases in the models at lower rates than the integrated water vapour associated with ARs (McClenny et al., 2020). As extreme precipitation increases with water vapour content (Emori & Brown, 2005; Kunkel et al., 2020), it is possible that there could be changes in extreme precipitation at higher rates than in the extreme IVT, with a consequent decrease in the simultaneous occurrence of extreme events of IVT and precipitation and a reduction in the importance of ARs as a major mechanism behind these concurrent extremes.

At this point, it is useful to make use of copulas to analyse carefully the influence that IVT has on extreme precipitation in the main regions of landfalling ARs (Figure 10, adapted from Fig. 1 in Algarra et al., 2020). For that purpose, we also used daily series of IVT and precipitation, but in this case they were averaged over the corresponding AR region. In Table 2, it is possible to find three metrics for each region for the whole period and for the two sub-periods:

a) The estimated probability of achieving a concurrent extreme of IVT and precipitation, computed using (7).

b) The estimated conditional probability of precipitation exceeding its corresponding 90th percentile, for a value of IVT equal to 250 $\mathrm{kg\,m^{-1}\,s^{-1}}$, computed using (8). This value represents a threshold commonly used to identify ARs (e.g., Ralph et al., 2019; Eiras-Barca et al., 2021).

c) The estimated value of IVT for which the probability of precipitation ex-

ceeding its corresponding 90th percentile equals 0.5.

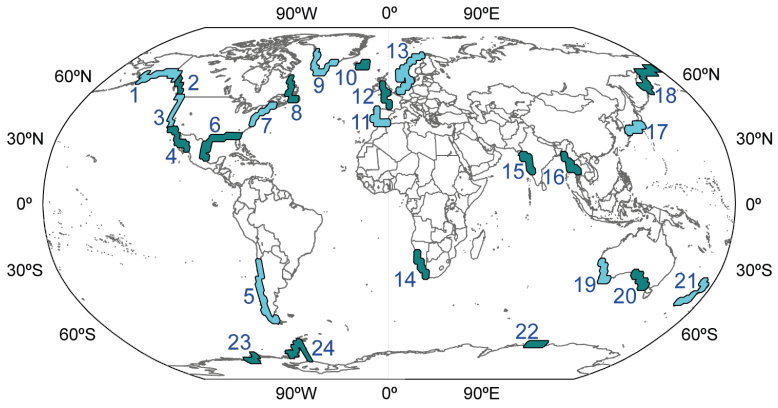

Figure 10: Regions of maximum occurrence of landfalling ARs adapted from Fig. 1 in Algarra et al. (2020).

Table 2: Results of the analysis of the IVT and precipitation averaged over the main AR regions. The metrics were calculated for the whole period 1981-2017, and the earlier and later studied periods, using the best fitted copula model in each case (according to the AIC). Please note that in this table, for simplicity, $P(.)$ refers to *estimated* probability.

REG.	SEASON	$P(Prec \geq q90_{prec},\ IVT \geq q90_{IVT})$			$P(Prec \geq q90_{prec} \mid IVT = 250)$			x s.t. $P(Prec \geq q90_{prec} \mid IVT = x) = 0.5$		
		whole	earlier period	later period	whole	earlier period	later period	whole	earlier period	later period
1	DJF	0.04	0.05	0.03	0.69	0.91	0.47	193.00	167.45	258.51
2	DJF	0.05	0.05	0.05	0.54	0.54	0.56	234.31	225.85	234.28
3	DJF	0.05	0.07	0.05	0.43	0.64	0.39	269.90	232.45	289.07
4	DJF	0.07	0.07	0.06	0.82	0.79	0.78	183.58	197.47	194.72
	JJA	0.03	0.02	0.03	0.35	0.25	0.41	343.85	339.09	343.85
5	JJA	0.03	0.03	0.03	0.59	0.72	0.44	223.51	201.87	263.21
6	DJF	0.03	0.04	0.03	0.18	0.21	0.17	454.07	388.88	535.51
	JJA	0.04	0.02	0.04	0.13	0.13	0.14	358.21	427.89	361.00
7	DJF	0.04	0.05	0.03	0.18	0.19	0.18	453.14	403.88	766.43
8	DJF	0.05	0.03	0.05	0.61	0.32	0.71	215.63	NaN	194.53
9	DJF	0.04	0.03	0.04	0.78	1.00	0.71	150.79	156.43	153.69
10	DJF	0.03	0.03	0.03	0.27	0.31	0.24	456.62	414.03	476.50
11	DJF	0.05	0.06	0.04	0.36	0.37	0.35	318.06	302.25	325.15
12	DJF	0.04	0.05	0.03	0.20	0.22	0.21	383.14	377.13	NaN
13	DJF	0.03	0.04	0.03	0.39	0.73	0.34	NaN	199.25	NaN
14	JJA	0.04	0.03	0.07	0.35	0.29	0.89	NaN	NaN	163.35
15	DJF	0.02	NA	NA	0.77	NA	NA	96.40	NA	NA
	JJA	0.04	0.02	0.05	0.03	0.03	0.04	680.09	1013.64	671.84
16	DJF	0.08	0.05	0.09	0.64	0.41	0.69	190.10	417.53	167.33
	JJA	0.03	0.03	0.03	0.04	0.04	0.05	800.26	794.70	767.69
17	DJF	0.04	0.04	0.05	0.32	0.30	0.33	333.35	338.23	328.32
18	DJF	0.04	0.04	0.04	0.83	1.00	0.80	133.79	127.00	123.12
19	JJA	0.04	0.05	0.04	0.31	0.33	0.28	402.70	343.42	NaN
20	JJA	0.03	0.04	0.03	0.29	0.34	0.23	NaN	NaN	NaN
21	JJA	0.05	0.05	0.04	0.51	0.63	0.40	248.81	213.20	284.57
22	JJA	0.05	0.04	0.05	0.34	0.59	0.35	NaN	171.02	NaN
23	JJA	0.03	0.05	0.00	0.90	0.52	0.06	164.56	90.11	NaN
24	JJA	0.03	0.03	0.03	0.94	0.94	0.97	188.17	133.06	143.41

NA (Not Available): The number of days of nonzero precipitation in the corresponding period is lower or equal to 400.
NaN (Not a Number): There is not a value x such that $P(Prec \geq q90_{prec} \mid IVT = x) = 0.5$ in the corresponding period.

These metrics were calculated for the corresponding winter of each AR region except for monsoonal regions, where both summer and winter were taken into account. The analysis of the whole period shows that in general terms, areas of ARs in the Northern Hemisphere have higher probabilities of achieving a concurrent extreme of IVT and precipitation than areas in the Southern Hemisphere, with maxima of 0.05 over the Pacific American coasts, The Canadian Atlantic, and the Iberian Peninsula, most of which are extratropical regions. In

the southern Hemisphere, the probabilities are higher in the Australian AR regions than in the American or African ones. In Polar AR regions, there are high probabilities of around 0.04 in the Northern Hemisphere but these are lower over the Antarctic AR regions, at around 0.02, the lowest among all the areas of AR landfall. AR monsoonal regions have moderate (around 0.03) probabilities of achieving a concurrent extreme of IVT and precipitation. These results have logical correspondence with the other two metrics: a) the lower probability of achieving a concurrent extreme of IVT and precipitation, b) the higher conditional probability of extreme precipitation for a value of IVT equal to 250 $\mathrm{kg\,m^{-1}\,s^{-1}}$, and c) the lower IVT for which the probability of precipitation exceeding its corresponding 90th percentile equals 0.5. We illustrate the meaning of these two metrics with an example. Region 3 (Californian coast) has a similar latitude to region 11 (Iberian Peninsula) and a lower latitude than region 1 (Alaska). For a day with a value of IVT of 250 $\mathrm{kg\,m^{-1}\,s^{-1}}$, which is typical of an AR, it is far more likely that the precipitation was extreme in California (43%) than in the Iberian Peninsula (36%), but much less likely than in Alaska (69%). Similarly, it is necessary to have a lower IVT in California (269.90 $\mathrm{kg\,m^{-1}\,s^{-1}}$) than in the Iberian Peninsula (318.08 $\mathrm{kg\,m^{-1}\,s^{-1}}$) but higher than in Alaska (193 $\mathrm{kg\,m^{-1}\,s^{-1}}$) to achieve a scenario where for two days of nonzero precipitation, one is an extreme precipitation day. This shows, again, that the strong latitudinal IVT gradient and the contrast from one region to another must be taken into account in the identification of ARs (Guan & Waliser, 2015; Reid et al., 2020), and in the characterisation of their strength and impacts (Ralph et al., 2019; Eiras-Barca et al., 2021).

The analysis of the three metrics by sub-period confirms the results presented in Figure 8. Almost all the AR regions with high or very high probabilities of concurrent extremes of IVT and precipitation (South Africa and Japan regions are the only exceptions) show a general tendency towards lower occurrence of simultaneous extremes in recent (warmer) periods. In one example in particular, for region 3 (California coasts) from the earlier period to the more recent warmer period, the estimated probability of achieving a concurrent extreme of

precipitation was reduced by half (0.07 to 0.04). In that region, the probability of a extreme precipitation day given an IVT of 250 $\mathrm{kg\,m^{-1}\,s^{-1}}$ was reduced from 64% to 39% and it is necessary to have about 67 $\mathrm{kg\,m^{-1}\,s^{-1}}$ of IVT to achieve a scenario where for two days of nonzero precipitation, one is an extreme precipitation day. An IVT of 250 $\mathrm{kg\,m^{-1}\,s^{-1}}$ implies a near certainty of extreme precipitation in Northern Hemisphere polar regions in the earlier period but not in the more recent (warmer) period. In any of the regions of higher AR occurrence, such as the Atlantic European coast, we estimated that only about one third of the days with this IVT value were associated with extreme precipitation in the recent (warmer) period.

4.3. Additional comments on the statistical analysis.

The statistical analysis of this study was mainly performed using the *R* package *VineCopula* (Nagler et al., 2020). The code used to obtain the results presented in this article is available from the authors upon reasonable request.

When using copulas, it is advisable to assess the impact that the autocorrelation between the observations has on the results. In our study, for each grid point, we repeated the statistical analysis selecting every third observation of the series, and the same was done for every fifth observation, in a similar way to Naveau et al. (2016). The results remained essentially unchanged from using the complete series, so we decided to keep all the observations in order to have a larger sample.

We also investigated the effect that the trend of the IVT and precipitation series had on our analysis. Both the IVT and precipitation series were linearly detrended and the results were completely analogous to the ones obtained for the non-detrended series, so we also opted to keep the original data.

For the copula models that were used to compute the metrics in Table 2, a Cramér–von Mises goodness-of-fit test was performed in each case (see Genest et al., 2009), by means of the *R* package *gofCopula* (Okhrin et al., 2020). The null hypothesis that the copula model fits well to the data was not rejected at significance level 0.05 in all the cases. Therefore, we can conclude that those

models were appropriate for the calculations that were carried out.

5. Conclusions

This paper offers an analysis of the concurrent extremes of vertically integrated water vapour transport (a local measure of moisture transport) and precipitation, the main aim being an understanding of the role played by atmospheric rivers, and whether this role has changed in the current warming climate.

The main conclusions reached in this work can be summarised in five main points, as follows:

- Copula models were a very useful tool for the analysis of the concurrent extremes of IVT and precipitation. On the one hand, for the worldwide analysis at grid-point level, they enabled us to estimate the probability of simultaneous occurrence of extreme values of the variables. On the other hand, for the in-depth analysis in the AR regions, we also made use of copulas to calculate two additional metrics: the estimated conditional probability of extreme precipitation for a value of IVT which represents a threshold commonly used to identify ARs, and the estimated value of IVT that is necessary to reach a scenario in which for two days of nonzero precipitation, one is an extreme precipitation day.

- The pattern of the absolute number of concurrent extremes of IVT and precipitation is very similar to the one corresponding to wind and precipitation: low in the tropics and growing in subtropical and extratropical regions, reaching its highest values along the coast of the continents in regions where atmospheric rivers occur. It is also possible to recognize the regional action of other meteorological structures associated with strong moisture transport, such as low-level jets or tropical cyclones.

- The estimated probability of achieving a concurrent extreme of IVT and precipitation shows a similar pattern to the one corresponding to the ab-

solute number of concurrent extremes, but intensifies as the number of precipitation days reduces. This is visible in the high probabilities in monsoonal areas during the dry season or the north-south gradient of probability in the regions of occurrence of ARs. Simultaneous high probabilities of occurrence of concurrent extremes together with moderately high values of IVT and precipitation occur mostly in regions of landfalling ARs.

- AR occurrence accounts for most of the concurrent extreme days of IVT and precipitation. Percentages of AR occurrence with respect to the concurrent extreme days reach values close to 90% in some seasons of the year in almost all the known regions of maximum occurrence of ARs, with percentages greater than 70% downwind of AR landfalling regions. This coincidence is low in tropical regions and in particular in monsoonal areas, with percentages lower than 50%. A careful copula-based analysis performed in the regions of maximum occurrence of landfalling ARs confirms that in Northern Hemisphere AR areas there are higher probabilities of achieving a concurrent extreme of IVT and precipitation than in the AR regions in the Southern Hemisphere. Moreover, the analysis enabled us to find that absolute maxima of probability occur over the Pacific American coasts, the Canadian Atlantic and the Iberian Peninsula, that only moderate probabilities occur over AR monsoonal regions, and that these are low over Antarctic AR regions.

- The role of ARs as drivers of concurrent extremes of IVT and precipitation is not the same for the two sub-periods of the study, one earlier and another more recent (warmer) period. The general tendency is towards a decrease in the influence of ARs in recent (warmer) periods, which is especially marked over the Pacific and Atlantic North American coasts during winter. This is evident both from the percentage of concurrent extreme days of IVT and precipitation that coincide with the occurrence of ARs and from the analysis of three copula-derived metrics.

This study has some limitations associated with i) the quality of the precipitation data, mainly associated with the density of the gauge network, this being particularly poor over tropical Africa and Antarctica; ii) the coarse resolution of the data of the reanalysis, which precludes a detailed regional analysis in areas with complex orography or where small-scale convective processes are relevant; iii) the definition of the concurrent extremes, herein the local 90th percentile, which is low compared with the 99th percentile more commonly used to define very rare extremes, but necessary in our case to permit large enough samples to relate seasonality to AR occurrence.

As suggested by Zscheischler et al. (2021), studies based on reanalysis should be compared with others using higher resolution models when compound precipitation and wind (in our case IVT) extremes are studied over complex terrain. This is the object of our further research, where a twofold nesting WRF simulation will be used to study the concurrent extremes of IVT and precipitation for current and future climates at a 6-km resolution for Western European coasts, a region of high AR occurrence.

Acknowledgements

Both authors acknowledge the financial support received from the Spanish Government within the LAGRIMA project (Grant No. RTI2018-095772-B-I00) and the partial support obtained from the Xunta de Galicia under Project ED431C 2017/64-GRC Programa de Consolidación e Estructuración de Unidades de Investigación Competitivas (Grupos de Referencia Competitiva) and Consellería de Educación e Ordenación Universitaria, both co-funded by the ERDF, in the framework of the Operational Program Galicia 2014–2020. The authors also acknowledge Bin Guan and Iago Algarra for providing data necessary for this research.

References

Akaike, H. (1974). A new look at the statistical model identification. *IEEE transactions on automatic control*, *19*, 716–723.

Algarra, I., Eiras-Barca, J., Nieto, R., & Gimeno, L. (2019). Global climatology of nocturnal low-level jets and associated moisture sources and sinks. *Atmospheric Research*, *229*, 39–59.

Algarra, I., Nieto, R., Ramos, A. M., Eiras-Barca, J., Trigo, R. M., & Gimeno, L. (2020). Significant increase of global anomalous moisture uptake feeding landfalling atmospheric rivers. *Nature communications*, *11*, 1–7.

Bao, J., Sherwood, S. C., Alexander, L. V., & Evans, J. P. (2017). Future increases in extreme precipitation exceed observed scaling rates. *Nature Climate Change*, *7*, 128–132.

Beck, H. E., Wood, E. F., Pan, M., Fisher, C. K., Miralles, D. G., Van Dijk, A. I., McVicar, T. R., & Adler, R. F. (2019). MSWEP V2 global 3-hourly 0.1 precipitation: methodology and quantitative assessment. *Bulletin of the American Meteorological Society*, *100*, 473–500.

Bevacqua, E., Maraun, D., Vousdoukas, M. I., Voukouvalas, E., Vrac, M., Mentaschi, L., & Widmann, M. (2019). Higher probability of compound flooding from precipitation and storm surge in Europe under anthropogenic climate change. *Science Advances*, *5*, eaaw5531.

Braz, D. F., Ambrizzi, T., Da Rocha, R. P., Algarra, I., Nieto, R., & Gimeno, L. (2021). Assessing the moisture transports associated with nocturnal low-level jets in continental South America. *Frontiers in Environmental Science*, .

Castillo, R., Nieto, R., Drumond, A., & Gimeno, L. (2014). The role of the ENSO cycle in the modulation of moisture transport from major oceanic moisture sources. *Water Resources Research*, *50*, 1046–1058.

Catto, J. L., & Dowdy, A. (2021). Understanding compound hazards from a weather system perspective. *Weather and Climate Extremes*, *32*, 100313.

Cong, R.-G., & Brady, M. (2012). The interdependence between rainfall and temperature: copula analyses. *The Scientific World Journal*, *2012*.

De Vries, A. J. (2021). A global climatological perspective on the importance of Rossby wave breaking and intense moisture transport for extreme precipitation events. *Weather and Climate Dynamics*, *2*, 129–161.

Dee, D. P., Uppala, S., Simmons, A., Berrisford, P., Poli, P., Kobayashi, S., Andrae, U., Balmaseda, M., Balsamo, G., Bauer, d. P. et al. (2011). The ERA-Interim reanalysis: Configuration and performance of the data assimilation system. *Quarterly Journal of the Royal Meteorological Society*, *137*, 553–597.

Dettinger, M. D., Ralph, F. M., & Lavers, D. A. (2015). Setting the stage for a global science of atmospheric rivers. *EOS, Earth and Space Science News*, *96*.

Dietzsch, F., Andersson, A., Ziese, M., Schröder, M., Raykova, K., Schamm, K., & Becker, A. (2017). A global ETCCDI-based precipitation climatology from satellite and rain gauge measurements. *Climate*, *5*, 9.

Drumond, A., Stojanovic, M., Nieto, R., Vicente-Serrano, S. M., & Gimeno, L. (2019). Linking anomalous moisture transport and drought episodes in the IPCC reference regions. *Bulletin of the American Meteorological Society*, *100*, 1481–1498.

Eiras-Barca, J., Ramos, A. M., Algarra, I., Vázquez, M., Dominguez, F., Miguez-Macho, G., Nieto, R., Gimeno, L., Taboada, J., & Ralph, F. M. (2021). European West Coast atmospheric rivers: A scale to characterize strength and impacts. *Weather and Climate Extremes*, *31*, 100305.

Emori, S., & Brown, S. (2005). Dynamic and thermodynamic changes in mean and extreme precipitation under changed climate. *Geophysical Research Letters*, *32*.

Espinoza, V., Waliser, D. E., Guan, B., Lavers, D. A., & Ralph, F. M. (2018). Global analysis of climate change projection effects on atmospheric rivers. *Geophysical Research Letters*, *45*, 4299–4308.

Genest, C., Rémillard, B., & Beaudoin, D. (2009). Goodness-of-fit tests for copulas: A review and a power study. *Insurance: Mathematics and economics*, *44*, 199–213.

Gimeno, L., Algarra, I., Eiras-Barca, J., Ramos, A. M., & Nieto, R. (2021). Atmospheric river, a term encompassing different meteorological patterns. *Wiley Interdisciplinary Reviews: Water*, (p. e1558).

Gimeno, L., Dominguez, F., Nieto, R., Trigo, R., Drumond, A., Reason, C. J., Taschetto, A. S., Ramos, A. M., Kumar, R., & Marengo, J. (2016). Major mechanisms of atmospheric moisture transport and their role in extreme precipitation events. *Annual Review of Environment and Resources*, *41*, 117–141.

Gimeno, L., Drumond, A., Nieto, R., Trigo, R. M., & Stohl, A. (2010). On the origin of continental precipitation. *Geophysical Research Letters*, *37*.

Gimeno, L., Nieto, R., Vázquez, M., & Lavers, D. A. (2014). Atmospheric rivers: A mini-review. *Frontiers in Earth Science*, *2*, 2.

Gimeno, L., Stohl, A., Trigo, R. M., Dominguez, F., Yoshimura, K., Yu, L., Drumond, A., Durán-Quesada, A. M., & Nieto, R. (2012). Oceanic and terrestrial sources of continental precipitation. *Reviews of Geophysics*, *50*.

Gimeno, L., Vázquez, M., Eiras-Barca, J., Sorí, R., Stojanovic, M., Algarra, I., Nieto, R., Ramos, A. M., Durán-Quesada, A. M., & Dominguez, F. (2020). Recent progress on the sources of continental precipitation as revealed by moisture transport analysis. *Earth-Science Reviews*, *201*, 103070.

Guan, B., & Waliser, D. E. (2015). Detection of atmospheric rivers: Evaluation and application of an algorithm for global studies. *Journal of Geophysical Research: Atmospheres*, *120*, 12514–12535.

Haberlandt, U. (2007). Geostatistical interpolation of hourly precipitation from rain gauges and radar for a large-scale extreme rainfall event. *Journal of Hydrology*, *332*, 144–157.

Held, I. M., & Soden, B. J. (2006). Robust responses of the hydrological cycle to global warming. *Journal of Climate*, *19*, 5686–5699.

Hersbach, H., Bell, B., Berrisford, P., Hirahara, S., Horányi, A., Muñoz-Sabater, J., Nicolas, J., Peubey, C., Radu, R., Schepers, D. et al. (2020). The ERA5 global reanalysis. *Quarterly Journal of the Royal Meteorological Society*, *146*, 1999–2049.

Joe, H. (2014). *Dependence modeling with copulas*. CRC Press.

Kim, H.-M., Zhou, Y., & Alexander, M. A. (2019). Changes in atmospheric rivers and moisture transport over the Northeast Pacific and western North America in response to ENSO diversity. *Climate Dynamics*, *52*, 7375–7388.

Kunkel, K. E., Stevens, S. E., Stevens, L. E., & Karl, T. R. (2020). Observed climatological relationships of extreme daily precipitation events with precipitable water and vertical velocity in the contiguous United States. *Geophysical Research Letters*, *47*, e2019GL086721.

Lavers, D. A., & Villarini, G. (2015). The contribution of atmospheric rivers to precipitation in Europe and the United States. *Journal of Hydrology*, *522*, 382–390.

Lazoglou, G., & Anagnostopoulou, C. (2019). Joint distribution of temperature and precipitation in the Mediterranean, using the Copula method. *Theoretical and Applied Climatology*, *135*, 1399–1411.

Liu, B., Tan, X., Gan, T. Y., Chen, X., Lin, K., Lu, M., & Liu, Z. (2020). Global atmospheric moisture transport associated with precipitation extremes: Mechanisms and climate change impacts. *Wiley Interdisciplinary Reviews: Water*, *7*, e1412.

Liu, Q., Li, T., & Zhou, W. (2021). Impacts of multi-timescale circulations on meridional moisture transport. *Journal of Climate*, *34*, 8065–8085.

Martius, O., Pfahl, S., & Chevalier, C. (2016). A global quantification of compound precipitation and wind extremes. *Geophysical Research Letters*, *43*, 7709–7717.

Massoud, E., Espinoza, V., Guan, B., & Waliser, D. (2019). Global climate model ensemble approaches for future projections of atmospheric rivers. *Earth's Future*, *7*, 1136–1151.

Mazdiyasni, O., & AghaKouchak, A. (2015). Substantial increase in concurrent droughts and heatwaves in the United States. *Proceedings of the National Academy of Sciences*, *112*, 11484–11489.

McClenny, E. E., Ullrich, P. A., & Grotjahn, R. (2020). Sensitivity of atmospheric river vapor transport and precipitation to uniform sea surface temperature increases. *Journal of Geophysical Research: Atmospheres*, *125*, e2020JD033421.

Messmer, M., & Simmonds, I. (2021). Global analysis of cyclone-induced compound precipitation and wind extreme events. *Weather and Climate Extremes*, *32*, 100324.

Mukherjee, S., & Mishra, A. K. (2021a). Cascading effect of meteorological forcing on extreme precipitation events: Role of atmospheric rivers in southeastern US. *Journal of Hydrology*, *601*, 126641.

Mukherjee, S., & Mishra, A. K. (2021b). Increase in compound drought and heatwaves in a warming world. *Geophysical Research Letters*, *48*, e2020GL090617.

Nagler, T., Schepsmeier, U., Stoeber, J., Brechmann, E. C., Graeler, B., & Erhardt, T. (2020). *VineCopula: Statistical Inference of Vine Copulas*. URL: `https://CRAN.R-project.org/package=VineCopula` R package version 2.4.1.

Naveau, P., Huser, R., Ribereau, P., & Hannart, A. (2016). Modeling jointly low, moderate, and heavy rainfall intensities without a threshold selection. *Water Resources Research*, *52*, 2753–2769.

Nayak, M. A., & Villarini, G. (2018). Remote sensing-based characterization of rainfall during atmospheric rivers over the central United States. *Journal of Hydrology*, *556*, 1038–1049.

Neiman, P. J., Ralph, F. M., Wick, G. A., Lundquist, J. D., & Dettinger, M. D. (2008). Meteorological characteristics and overland precipitation impacts of atmospheric rivers affecting the West Coast of North America based on eight years of SSM/I satellite observations. *Journal of Hydrometeorology*, *9*, 22–47.

Nelsen, R. B. (2006). *An introduction to copulas*. Springer Science & Business Media.

Nie, J., Sobel, A. H., Shaevitz, D. A., & Wang, S. (2018). Dynamic amplification of extreme precipitation sensitivity. *Proceedings of the National Academy of Sciences*, *115*, 9467–9472.

Okhrin, O., Trimborn, S., & Waltz, M. (2020). gofCopula: Goodness-of-Fit Tests for Copulae. *Discussion Paper*, . URL: `https://papers.ssrn.com/sol3/papers.cfm?abstract_id=3560825`.

Owen, L. E., Catto, J. L., Stephenson, D. B., & Dunstone, N. J. (2021). Compound precipitation and wind extremes over Europe and their relationship to extratropical cyclones. *Weather and Climate Extremes*, *33*, 100342.

Payne, A. E., Demory, M.-E., Leung, L. R., Ramos, A. M., Shields, C. A., Rutz, J. J., Siler, N., Villarini, G., Hall, A., & Ralph, F. M. (2020). Responses and impacts of atmospheric rivers to climate change. *Nature Reviews Earth & Environment*, *1*, 143–157.

Ralph, F. M., Cordeira, J. M., Neiman, P. J., & Hughes, M. (2016). Landfalling atmospheric rivers, the Sierra Barrier Jet, and extreme daily precipitation in

northern California's upper Sacramento River watershed. *Journal of Hydrometeorology*, *17*, 1905–1914.

Ralph, F. M., & Dettinger, M. D. (2011). Storms, floods, and the science of atmospheric rivers. *EOS, Transactions American Geophysical Union*, *92*, 265–266.

Ralph, F. M., Dettinger, M. D., Cairns, M. M., Galarneau, T. J., & Eylander, J. (2018). Defining "atmospheric river": How the Glossary of Meteorology helped resolve a debate. *Bulletin of the American Meteorological Society*, *99*, 837–839.

Ralph, F. M., Neiman, P. J., Wick, G. A., Gutman, S. I., Dettinger, M. D., Cayan, D. R., & White, A. B. (2006). Flooding on California's Russian River: Role of atmospheric rivers. *Geophysical Research Letters*, *33*.

Ralph, F. M., Rutz, J. J., Cordeira, J. M., Dettinger, M., Anderson, M., Reynolds, D., Schick, L. J., & Smallcomb, C. (2019). A scale to characterize the strength and impacts of atmospheric rivers. *Bulletin of the American Meteorological Society*, *100*, 269–289.

Reddy, M. J., & Ganguli, P. (2012). Bivariate flood frequency analysis of Upper Godavari River flows using Archimedean copulas. *Water Resources Management*, *26*, 3995–4018.

Reid, K. J., King, A. D., Lane, T. P., & Short, E. (2020). The sensitivity of atmospheric river identification to integrated water vapor transport threshold, resolution, and regridding method. *Journal of Geophysical Research: Atmospheres*, *125*, e2020JD032897.

Rutz, J. J., Steenburgh, W. J., & Ralph, F. M. (2015). The inland penetration of atmospheric rivers over western North America: A Lagrangian analysis. *Monthly Weather Review*, *143*, 1924–1944.

Salvadori, G., & De Michele, C. (2004). Frequency analysis via copulas: Theoretical aspects and applications to hydrological events. *Water resources research*, *40*.

Shemyakin, A., & Kniazev, A. (2017). *Introduction to Bayesian estimation and copula models of dependence*. Wiley Online Library.

Sklar, M. (1959). Fonctions de repartition an dimensions et leurs marges. *Publ. Inst. Statist. Univ. Paris*, *8*, 229–231.

Sun, Y., Solomon, S., Dai, A., & Portmann, R. W. (2006). How often does it rain? *Journal of Climate*, *19*, 916–934.

Tan, Y., Yang, S., Zwiers, F., Wang, Z., & Sun, Q. (2021). Moisture budget analysis of extreme precipitation associated with different types of atmospheric rivers over western north america. *Climate Dynamics*, (pp. 1–17).

Tarek, M., Brissette, F. P., & Arsenault, R. (2020). Evaluation of the ERA5 reanalysis as a potential reference dataset for hydrological modelling over North America. *Hydrology and Earth System Sciences*, *24*, 2527–2544.

Trenberth, K., Zhang, R. et al. (2021). The Climate Data Guide: Atlantic Multi-decadal Oscillation (AMO). Last modified 05 Jun 2021. Retrieved from https://climatedataguide.ucar.edu/climate-data/atlantic-multi-decadal-oscillation-amo.

van der Ent, R. J., & Savenije, H. H. (2013). Oceanic sources of continental precipitation and the correlation with sea surface temperature. *Water Resources Research*, *49*, 3993–4004.

van der Ent, R. J., Savenije, H. H., Schaefli, B., & Steele-Dunne, S. C. (2010). Origin and fate of atmospheric moisture over continents. *Water Resources Research*, *46*.

Vázquez, M., Nieto, R., Liberato, M. L., & Gimeno, L. (2020). Atmospheric moisture sources associated with extreme precipitation during the peak precipitation month. *Weather and Climate Extremes*, *30*, 100289.

Wahl, T., Jain, S., Bender, J., Meyers, S. D., & Luther, M. E. (2015). Increasing risk of compound flooding from storm surge and rainfall for major US cities. *Nature Climate Change*, *5*, 1093–1097.

Waliser, D., & Guan, B. (2017). Extreme winds and precipitation during landfall of atmospheric rivers. *Nature Geoscience*, *10*, 179–183.

Xie, P., Chen, M., Yang, S., Yatagai, A., Hayasaka, T., Fukushima, Y., & Liu, C. (2007). A gauge-based analysis of daily precipitation over East Asia. *Journal of Hydrometeorology*, *8*, 607–626.

Xiong, Y., & Ren, X. (2021). Influences of Atmospheric Rivers on North Pacific Winter Precipitation: Climatology and Dependence on ENSO Condition. *Journal of Climate*, *34*, 277–292.

Xu, X., Frey, S. K., Boluwade, A., Erler, A. R., Khader, O., Lapen, D. R., & Sudicky, E. (2019). Evaluation of variability among different precipitation products in the Northern Great Plains. *Journal of Hydrology: Regional Studies*, *24*, 100608.

Zhu, Y., & Newell, R. E. (1994). Atmospheric rivers and bombs. *Geophysical Research Letters*, *21*, 1999–2002.

Zscheischler, J., Naveau, P., Martius, O., Engelke, S., & Raible, C. C. (2021). Evaluating the dependence structure of compound precipitation and wind speed extremes. *Earth System Dynamics*, *12*, 1–16.

Zscheischler, J., & Seneviratne, S. I. (2017). Dependence of drivers affects risks associated with compound events. *Science Advances*, *3*, e1700263.